Theoretical Study of the Reductive Decomposition of Ethylene Sulfite: A Film-Forming Electrolyte Additive in Lithium Ion Batteries

ARTICLE *in* THE JOURNAL OF PHYSICAL CHEMISTRY A · OCTOBER 2012

Impact Factor: 2.69 · DOI: 10.1021/jp3081996 · Source: PubMed

2 AUTHORS:

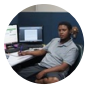

Ermias Girma Leggesse
National Taiwan University of Science and Tec…
19 PUBLICATIONS **38** CITATIONS
SEE PROFILE

Jyh-Chiang Jiang
National Taiwan University of Science and Tec…
174 PUBLICATIONS **2,612** CITATIONS
SEE PROFILE

THE JOURNAL OF PHYSICAL CHEMISTRY A

Article

pubs.acs.org/JPCA

Theoretical Study of the Reductive Decomposition of Ethylene Sulfite: A Film-Forming Electrolyte Additive in Lithium Ion Batteries

Ermias Girma Leggesse and Jyh-Chiang Jiang*

Department of Chemical Engineering, National Taiwan University of Science and Technology, Taipei, 106, Taiwan, R.O.C

Supporting Information

ABSTRACT: The role of ethylene sulfite (ES) as an electrolyte additive for lithium ion batteries is explained by investigating the one- and two-electron reductive decomposition of ES and (ES)$Li^+(PC)_n$ (n = 0−2), both in vacuum and solvent, with the aid of high-level density functional theory calculations. The open-chain radical, which is formed as a result of reduction of ES in solvent without first being coordinated with Li^+, is further stabilized by a dissolved lithium ion. The resulting more stable intermediate releases a somewhat large amount of energy, which is utilized in the formation of a subsequent radical anion. On the basis of the study on the reductive decomposition of ES, (ES)$Li^+(PC)$, and (ES)$Li^+(PC)_2$, the major products that are responsible for the formation of a protective solid electrolyte interphase film are Li_2SO_3, $(CH_2OSO_2Li)_2$, $CH_3CH(OSO_2Li)CH_2OCO_2Li$, and $ROSO_2Li$.

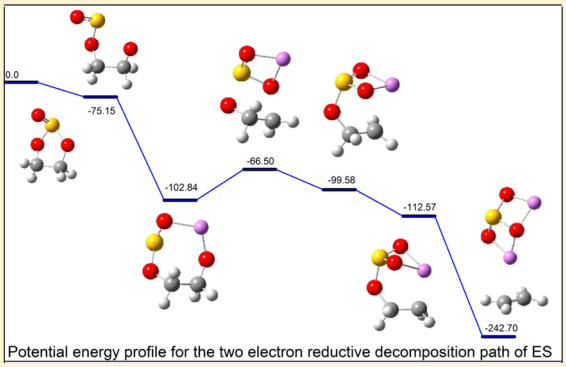

Potential energy profile for the two electron reductive decomposition path of ES

INTRODUCTION

Lithium ion batteries offer various advantages compared to other types of rechargeable batteries, including high energy density, flexible and lightweight design, and a longer lifespan than comparable battery technologies.[1−4] They exhibit major advantages for hybrid electric vehicles (HEVs) and plug-in hybrid electric vehicles (PHEVs), along with other applications.[5] As a result of this, they are being considered as a leading contender for a clean and sustainable energy source.

A typical lithium ion battery system is made up of a graphitic carbon as the anode, a transition-metal oxide as the cathode, and nonaqueous organic electrolytes that are based on solutions of one or more lithium salts in a mixture of two or more solvents. Among the wide spectrum of polar solvents, cyclic diesters of carbonic acid have attracted lots of research attention especially after their role in the formation of a protective film on the graphite electrode was recognized.[6] This film, which was first named the "solid electrolyte interphase" (SEI) by Peled,[7] lies between the electrode and the electrolyte solution, and it is conductive to lithium ions but nonconductive to electrons. As the SEI layer highly determines some of the critical properties of the lithium ion battery such as safety, cyclability, and power capability, the study of its formation process and morphology became one of the key areas of research in the performance development of lithium ion batteries.

Propylene carbonate (PC) exhibits remarkable properties because of its ability to dissolve and dissociate lithium salts, leading to electrolytes having high ionic conductivity over a wide temperature range.[8,9] Moreover, its high dielectric constant and stability with lithium makes it the most popular solvent that is widely used in lithium ion batteries. However, PC can easily decompose on graphite and co-insert with a Li ion into a graphite electrode, which results in the destruction of the graphite electrode and reduces its reversible capacity.[10−16] Because the intercalation of a lithium ion into graphite occurs at low potentials (below 0.25 V versus Li/Li^+), the relative solvents and salts are partially reduced to form SEI on the surface of a graphite electrode, which is associated with irreversible capacity loss.[17−19] Many methods have been reported to suppress the intercalation of the solvent into graphite. One method is by using proper electrolyte additives, which would help to generate an efficient SEI layer.

In recent years, sulfur-based additives including SO_2, CS_2, and cyclic sulfites (such as ethylene sulfite (ES), propylene sulfite, and aryl sulfites) have been reported to facilitate the formation of SEI when present in a small amount together with PC or a mixture of PC and other solvents.[20−27] Organic sulfites such as ES have been found to be a good SEI film-forming additive for lithium ion batteries containing PC as a solvent.[27−30] Gerhard H. Wrodnigg et al. introduced the solvent ES as an additive for PC-based electrolyte in a lithium ion battery and found that even a small volume fraction of 5 vol % ES successfully suppresses PC co-intercalation into graphite with promising low-temperature performance.[30] However, there are very few reported studies about the mechanism by which these additives promote the formation of a stable SEI layer on the anode material.[22,31] Very recently, Xing et al.[22] tried to investigate the reduction mechanism of ES by considering only gas-phase DFT calculations. However, they

Received: August 17, 2012
Revised: October 2, 2012
Published: October 18, 2012

   dx.doi.org/10.1021/jp3081996 | J. Phys. Chem. A 2012, 116, 11025−11033

did not address the implicit and explicit solvent effect that will have a pronounced effect on how ES will perform in the electrolyte system under investigation.

In this paper, high-level density functional theory calculations have been carried out to carefully analyze the role of ES as a SEI-forming additive, starting with the electroreductive decomposition of ES in the gas phase and then taking into account the solvent effect with the supermolecular models $(ES)Li^+(PC)_n$ (n = 0−2).

COMPUTATIONAL DETAILS

All geometry optimizations and frequency determinations were performed using the Gaussian 09 package.[32] Density functional theory (DFT) method has been applied because of its favorable balance between accuracy and computational efficiency. A widely used B3LYP, which is a hybrid functional, comprised of the Becke's three-parameter exact exchange functional (B3) in conjunction with the nonlocal gradient-corrected correlation functional of Lee−Yang−Parr (LYP)[33−36] has been used with the triple split valence basis set 6-311G along with a set of d,p polarization functions on heavy atoms and hydrogen atoms.[37] Recently, theoretical and computational studies on lithium ion battery electrolyte systems employing the above level of theory have been reported.[22,38−43] A spin-unrestricted scheme was used for the odd numbers of electron systems to allow for any possible bond cleavage during geometry optimization.

To confirm the transition states and make zero-point energy (ZPE) corrections, frequency analyses are done with the same basis sets as those for the geometry optimization. Intrinsic reaction coordinate (IRC) calculations were also performed to confirm whether the reaction path of the respective chemical reaction correctly connects the stationary points under consideration. Unless otherwise stated, the relative energies indicate those with ZPE correction, and Gibbs free energies and enthalpies are calculated at 298.15 K. The spin contamination was considered by comparison of the expectation value of the $\langle S^2\rangle$ operator. $\langle S^2\rangle$ before annihilation was mostly between 0.75 and 0.77 for the doublet states, confirming that the spin contamination would have an insignificant effect on the result. Natural bond orbital (NBO)[44] analysis with the same basis set was performed with the NBO program included in the Gaussian program package.

To examine the solvent effects, specific solvent molecules are explicitly included in the calculations with the molecular clusters $(PC)_nLi^+(ES)$ (n = 1, 2) in a vacuum. The implicit solvent effect was accounted for by using the polarized continuum model (PCM)[45] in which a conventional set of Pauling radii and 70 tesserae has been used for all calculations. We adopted the dielectric constant of PC (64.9) in relation to the conditions implemented in experiments. The bonding characteristics between lithium and the solvent molecules were investigated by using Bader's atoms in molecules (AIM) theory.[46] In the present work, we used the electron density function $\rho(r)$ and its Laplacian $\nabla^2\rho(r)$ to elucidate the structural results and bonding properties at the bond critical points (bcp's).

RESULTS AND DISCUSSION

Reduction Mechanism of ES in Vacuum and Bulk Solvent. The calculated solvation energies, frontier molecular orbital energies, and vertical electron affinities (EA_v) of ES and PC in vacuum and bulk solvent are listed in Table 1. Vertical electron affinities can be defined as the energy difference between the neutral molecule and its negative ion at their initial geometry.[47] The calculated EA_v of ES (2.99 eV) is larger than PC (0.92 eV), implying the superior ability of ES to gain the first electron. The negative gas-phase EA_v value for PC implies that the neutral species is more stable than the anion. Moreover, the LUMO energy of ES (−1.27 eV) is lower than that of PC (−0.17 eV), indicating the readiness of ES to be reduced on the anode surface prior to PC. Thus, while ES can readily accept an electron in both the gas phase and solvent, PC is not a good electron acceptor in the gas phase. Compared to the neutral species of ES and PC, the anions are more solvated, as realized from the solvation free energy. This difference in solvation energy also contributes to the discrepancy in solution reduction potentials between PC and ES.

Table 1. Frontier Molecular Orbital Energy, Electron Affinity, and Energies of Solvation (eV) for PC and ES in Bulk Solvent and Vacuum

	frontier molecular orbital energy		EA_v[a]		ΔE_{solv}[b]	
molecule	E_{HOMO}	E_{LUMO}	in solution	in vacuum	neutral	anion
PC	−8.68	−0.17	0.92	−0.28	−0.35	−1.58
ES	−8.28	−1.22	2.99	0.95	−0.21	−2.25

[a] $EA_v = E(M_{optimized}) - E([M^-]_{optimized})$. [b] Solvation energy is defined as the difference between the energy of the species in solution minus that in vacuum.

To elucidate the mechanism of bond breaking in the ES electroreduction process, bond orders of ES (**1**) and $ES^{\bullet-}$ (**2**) were calculated using the natural population analysis with natural localized molecular orbitals (NLMO/NPA). The bond orders in Table 2 follow the trend of bond length change from **1** to **2**. The result indicates that after ES gains an electron, the O_4-S_1 bond is weakened, which is evident from the significant decrease of the corresponding bond order. On the basis of the bond order and structure analysis, it can be seen that ES experiences the braking of the O_4-S_1 bond to form an open-chain radical as a result of reduction.

Table 2. NLMO/NPA Bond Orders in ES and $ES^{\bullet-}$

	bond order	
bond	ES	$ES^{\bullet-}$
S1−O2	0.3495	0.3917
S1−O3	0.1968	0.2102
S1−O4	0.1934	0.1028
O3−C5	0.2161	0.2135
O4−C6	0.2169	0.2732
C5−C6	0.2545	0.2463

Figure 1 shows the selected geometrical parameters of the relevant species on the potential energy surface of the reductive decomposition of ES. The respective energies and Gibbs free energies, obtained at the B3LYP/6-311++G(d,p) and at PCM-B3LYP/6-311++G(d,p) levels, are collected in Table 3. The energy surface profile is also illustrated in Figure 2.

A population analysis on the spin density shows that the unpaired electron mainly locates on the sulfur atom in **2** with a coefficient of about 0.50, indicating that the reduction of ES took place on the sulfur atom. The open-chain anion radical **2** proceeds via a transition state **3** to give SO_2 and CH_2CHO. The

dx.doi.org/10.1021/jp3081996 | J. Phys. Chem. A 2012, 116, 11025−11033

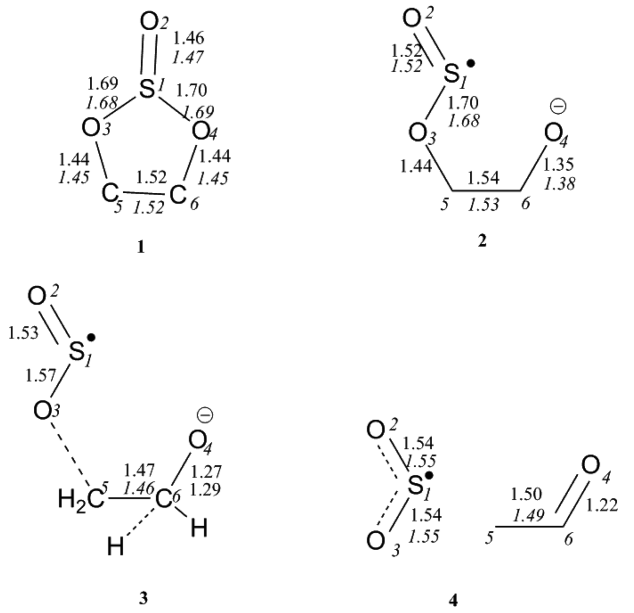

Figure 1. Optimized geometries from B3LYP/6-311++G(d,p). Data in italics are from PCM-B3LYP/6 311++G(d,p).

energy barrier for the formation of the products from **2** is lower in the gas phase than that in solvent (17.39 versus 27.79 kcal/mol), indicating a significant solvent effect in the product formation. This observation is in agreement with the speculation made by Robertson et al. in their study about interactions of free and quasi free electrons with ES.[48] By using both Rydberg electron transfer (RET) and dissociative electron attachment (DEA) measurements, they concluded that SO_2 is the most predominant species formed from electron attachment to ES, which results due to the cleavage of a C−O bond of ES as predicted in this work.

On the basis of these observation, one might suggest that SO_2 would further go through many electron reduction processes, as seen when SO_2 is used as an electrolyte additive, and result in the formation of passive layers comprised of a mixture of organic and inorganic Li salts such as Li-alkyl carbonates, $Li_2S_2O_4$, Li_2SO_3, and $Li_2S_2O_5$. However, contrary to what has been suggested by Xing et al.[22] in their study about the reductive mechanism of ethylene sulphite, SO_2 is not experimentally observed in a PC-based electrolyte containing ES.[30] The presence of SO_2 could have been detected via experimental measurements as a result of its reduction. However, Wrodnigg et al. showed that the SO_2 reduction on carbonaceous materials is reversible while the reduction reaction in the presence of ES as an electrolyte additive is apparently irreversible, which is attributed to the decomposition of the electrolyte solutions that are related to SEI

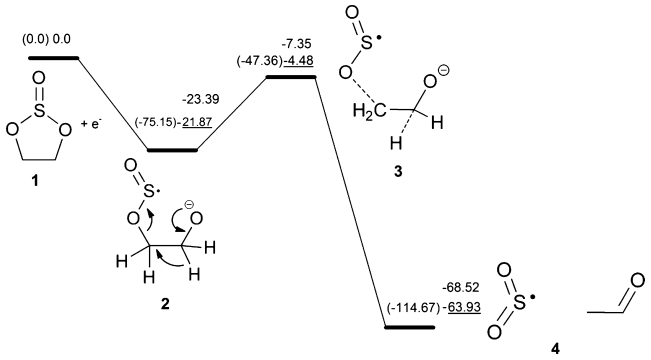

Figure 2. Potential energy (underlined data) and Gibbs free energy profile for reductive decomposition of ES calculated with B3LYP/6-311++G(d,p). The data in parentheses refer to relative energies calculated with PCM-B3LYP/6-311++G(d,p).

formation.[30] One possible explanation for this is the stabilization of the open-chain radical by Li^+ to form **7**, which is much more preferable than proceeding to give a SO_2 radical via a transition state **3**. Hence, after gaining one electron, the radical ion formed prefers to bind with Li^+ and undergo further electrochemical reactions, as discussed in the next sections.

Li^+ Solvation in ES Containing PC-Based Electrolyte Solutions. Because decomposition reactions in lithium ion batteries are strongly affected by lithium ion solvation, it is pragmatic to examine first the solvation of lithium ions in the electrolyte solutions. Table 4 summarizes the average Li^+−O bond distance, binding energy per species, Gibbs free energy, heat of formation, change in entropy of the system, and total atomic charges on Li^+ ions of the supermolecular clusters $(ES)_mLi^+(PC)_n$ (m = 0, 1 and n = 0−3). The average bond distance between lithium and oxygen increases with an increase in the number of PC molecules, which is accompanied by a decrease in the binding energy, probably due to repulsion among coordinated molecules. This observation is in agreement with a recent speculation by Wang et al. that the binding energy decreases as the number of PC molecules increases.[18] Furthermore, it was found that the positive charge on the lithium ion tends to decrease with n for a given solvent. This observation can be attributed to the wider distribution of the positive charge of lithium in space as the size of the solvated lithium ion increases.

The stripping of the solvation sheath of Li^+, which involves partial dissolution and anion formation on the electrode, is reported to be the major energy-consuming step in lithium ion batteries.[49−52] On the basis of this phenomenon, Park et al.[53] demonstrated that the low Li^+ ion binding affinity is an important characteristics of SEI-forming additives. The calculated Li^+ binding energy for ES is in the range of −46.44 to −19.46 kcal/mol, which is quite enough to propose

Table 3. Relative Energies,[a] Enthalpies, and Free Energies (in kcal/mol) of the Stationary Points, Charge of the Sulfur Atom, Spin Densities (SDs), and Imaginary Frequency (ω/cm^{-1}) for the ES Reduction Process Calculated with B3LYP/6-311++G(d,p)

structures	ΔE + ZPE	ΔH	ΔG	q	SD	ω
1	0	0	0	1.64	0	
2	−21.87 (−75.15)	−21.21	−23.38	1.06	0.50	
3 (TS, 2 ↔ 4)	−4.48 (−47.36)	−3.50	−7.35	1.06	0.55	−751
4	−63.93 (−114.67)	−61.99	−68.52	0.98	0.55	

[a]The data in the parentheses are from PCM-B3LYP/6-311++G(d,p).

dx.doi.org/10.1021/jp3081996 | J. Phys. Chem. A 2012, 116, 11025−11033

Table 4. Average Li^+−O Distance (r, Å), Binding Energies (BEs, kcal/mol), Heat of Reaction (ΔH, kcal/mol), Gibbs Free Energies of Reaction (ΔG, kcal/mol), Change in Entropy of the System (ΔS_{system}, kcal/(mol K)), and Charge on the Li^+ Ion (q) Calculated at the B3LYP/6-311++G(d,p) Level[a]

reactions	r	BE	ΔH	ΔG	ΔS	q
$Li^+ + PC \rightarrow Li^+(PC)$	1.73 (1.76)	−50.83 (−51.9)	−57.10 (−52.1)	−43.30 (−46.0)	−0.023	0.919
$Li^+ + ES \rightarrow Li^+(ES)$	1.75	−46.44	−45.81	−39.53	−0.025	0.985
$Li^+(PC) + PC \rightarrow Li^+(PC)_2$	1.79 (1.81)	−45.18 (−45.80)	−37.65 (−39.2)	−30.84 (−31.9)	−0.028	0.962
$Li^+(PC) + ES \rightarrow (ES)Li^+(PC)$	1.80/1.78	−34.46	−33.89	−25.73	−0.026	0.958
$Li^+(PC)_2 + ES \rightarrow (ES)Li^+(PC)_2$	1.88/1.85	−19.46	−18.82	−10.89	−0.027	0.929
$Li^+(PC)_3 + ES \rightarrow (ES)Li^+(PC)_3$		−12.21	−12.12	1.88	−0.046	0.887

[a]The data in parentheses are from ref 18, calculated at the B3PW91/6-31++G(d,p) level.

the existence of the salt effect in the system. The BE of $Li^+(ES)$ is lower than that of $Li^+(PC)$ by approximately 4.4 kcal/mol. Furthermore, the average distance between lithium and oxygen increases by 0.02 Å, indicating the weak binding nature of Li^+ with ES. Another reason for the preferential solvation of lithium ions by PC rather than ES can be ascribed to the presence of the methyl group, which induces an increase in the negative electric charge density on the oxygen of the carbonyl group of PC, resulting in stronger solvation to the lithium ion. Moreover, the stabilization of the molecular structure of PC by the formation of the Li^+−(PC) bonding can also be used as evidence for strong solvation of the Li^+ ion by PC. The PC ring is distorted with a O−C−C−O dihedral angle of 23°, which is relaxed by the formation of the Li^+−(PC) bond in which the O−C−C−O dihedral angle is reduced to 17°. However, a similar kind of structural change upon lithium coordination does not occur for ES (the corresponding dihedral angles are 37.45 and 37.68° before and after coordination, respectively). Thus, it is highly probable that the difference in the stabilization of solvent molecules by forming bonds with lithium ions contributes to the difference in ΔG between PC and ES, as shown in Table 4. This observation is also supported by the AIM calculations at the B3LYP/6-311++G(d,p) level for $Li^+(ES)$ and $Li^+(PC)$, in which $\rho(r)$ and its Laplacian $\nabla^2\rho(r)$ at the bcp between lithium and oxygen for $Li^+(PC)$ [$\rho(r) = 0.044$, $\nabla^2\rho(r) = 0.392$] are slightly higher than those for $Li^+(ES)$ [$\rho(r) = 0.042$, $\nabla^2\rho(r) = 0.371$].

For the reaction to form $(ES)Li^+(PC)_3$, we have found that both ΔH and ΔS_{system} are negative, which means that energy is given out from the system to the surroundings accompanied by a more ordered product formation. However, the Second Law of Thermodynamics tells us that a reaction is only possible if the entropy of the universe, which is the sum of the entropy of the system and surroundings, increases. This happens because the reaction gives out heat energy to the surroundings, as seen from the negative ΔH, which in turn increases the entropy of the surroundings to compensate for the entropy decrease of the system. It is essential to take account of the total entropy change of the system and the surroundings in order to predict the feasibility of a particular reaction. The change in entropy of the surroundings ($\Delta S_{surroundings} = -\Delta H/T$) for the reaction that gives $(ES)Li^+(PC)_3$ was found to be 0.040 kcal mol^{-1} K^{-1}; thus, the total entropy change ($\Delta S_{total} = \Delta S_{system} + \Delta S_{surroundings}$) brought about by the reaction is -6×10^{-3} kcal mol^{-1} K^{-1}. According to the Second Law of Thermodynamics, because ΔS_{total} for this reaction is negative, the formation of $(ES)Li^+(PC)_3$ will not be feasible. Furthermore, the positive ΔG value of $(ES)Li^+(PC)_3$ also affirms the above conclusion. Similarly, $\Delta S_{surroundings}$ and ΔS_{total} values for the reaction leading to the formation of $(ES)Li^+(PC)_2$ were calculated to be 0.063 and 0.036 kcal mol^{-1} K^{-1}, respectively, confirming the possibility of the formation of the product.

On the basis of the above discussion and from the calculated Gibbs free energies of formation for $Li^+(ES)$ ($\Delta G = -39.53$ kcal/mol), $(ES)Li^+(PC)$ ($\Delta G = -25.73$ kcal/mol), and $(ES)Li^+(PC)_2$ ($\Delta G = -10.89$ kcal/mol), it can be realized that $Li^+(ES)$, $(ES)Li^+(PC)$, and $(ES)Li^+(PC)_2$ are most likely the major solvated lithium ion species in ES-containing electrolytes, with the concentration of $(ES)Li^+(PC)_2$ being higher than that of $(ES)Li^+(PC)$. All of these results strongly suggest that in a PC-based electrolyte where ES is used as an additive, the maximum number of molecules that can solvate a Li^+ ion is three. This condition is analogous to a conclusion made by Wang et al.[18] for PC-containing electrolyte systems in which the formation of a four-coordinated Li^+ species was not favorable, which is also supported by electrospray ionization mass spectroscopy (ESI-MS) studies by Fukushima et al.[54−56] It is understandable that the solvation number of Li^+ depends on the steric effect of the respective solvent molecules. For example, the favorable solvation number of Li^+ has been studied by using Fourier transform ion cyclotron resonance spectrometry and reported to be 2 in diethylether and 3 in acetone and tetrahydrofuran.[57] Alternatively, it has been proposed that in less bulky solvent molecules like acetonitrile, the coordination number of the Li^+ ion would reach as high as 6.[58] Therefore, in the following sections, we will focus on discussing the reductive decomposition mechanisms of $Li^+(ES)$, $(ES)Li^+(PC)$, and $(ES)Li^+(PC)_2$, which are most likely the major solvated lithium ion species in the system under study.

Effect of Salt in One- and Two-Electron Reduction of ES. The nonaqueous electrolyte solution of lithium ion batteries is composed of strongly solvated Li^+ ions, weekly solvated salt anions, and isolated solvent molecules. The difference in solvation strength between Li^+ ions and the corresponding counterions can be ascribed to the smaller ionic radius of the former. Some of the competitive reactions that occur when the graphite electrode is cathodically polarized consist of co-intercalation of the solvation shells into the graphene layers, intercalation of Li^+ ions into graphene layers, and electron transfer from the graphite electrode to the solvent and salt anions. Among these reactions, in the current and proceeding sections, we will focus on the solvent co-intercalation systems that will decompose in the nonaqueous electrolyte solution near the edge sites of the graphite electrode.

Table 5 presents the relative energies for the two-electron reduction of ES and $Li^+(ES)$. Note that because there is no reported data for the solvation free energy of the electron in the electrolyte system that we are discussing, we have adapted the free energy of an electron in water and methanol in our calculation. This approach, to account for the free energy of the

Table 5. Relative Energies and Gibbs Free Energies (kcal/mol) for the Two-Electron Reduction of ES and Li^+(ES)

		ΔE	ΔG_{vac} [a]	ΔG_{sol} [b]
ES	5 + $2Li^+$ + $2e^-$	0.0	0.0	0.0
	6 + $2Li^+$ + e^-	−75.15	−23.39	−62.34 (54.96)
	7 + Li^+ + e^-	−102.84	−187.78	−246.96 (−239.58)
	8 + Li^+ + e^-	−66.50	−138.79	−161.76 (−154.38)
	9 + Li^+ + e^-	−99.58	−162.47	−229.09 (−221.71)
	10 + Li^+	−112.57	−213.27	−300.04 (−285.29)
	11	−242.70	−405.14	−562.21 (−547.46)
Li^+(ES)	22 + Li^+ + $2e^-$	0.0	0.0	0.0
	23 + Li^+ + e^-	−82.22	−148.02	−191.70 (−184.32)
	24 + Li^+ + e^-	−45.98	−99.04	−106.71 (−99.33)
	25 + Li^+ + e^-	−79.07	−131.49	−174.04 (−166.66)
	26 + Li^+	−92.05	−148.18	−118.79 (−275.27)
	27	−222.19	−333.86	−442.52 (−427.76)

[a] ΔG_{vac} stands for the relative Gibbs free energy in gas phase calculated with B3LYP/6-311++G(d,p). [b] ΔG_{sol} = ΔG_{vac} + relative solvation free energies, including −37.59 kcal/mol for the free energy of solvation of electron in H_2O (ε=80.20) and values in parentheses are calculated using −44.97 kcal/mol for the free energy of solvation of electron in CH_3O (ε=33.0) from reference 59.

electron, has also been used by Vollmer et al.[59] in their study about the reduction mechanism of EC, PC, and VEC. When going from the isolated reactants to the products, the change in solution free energy (ΔG_{sol}) increases as compared to the gas-phase free energies of the reaction species (ΔG_{vac}). This is due to the significant contribution from solvation energies of the lithium ion and the free electrons in the solution. The relative stabilities of the products have also increased as a result of a major contribution from the solvation, which makes the reactions less exoergic.

The two-electron reduction mechanism (similar to the high current density) of ES, which leads to the formation of Li_2SO_3 and alkene, is shown in Scheme 1, and its energy surface profile

Scheme 1. Two-Electron Reduction Mechanism of ES

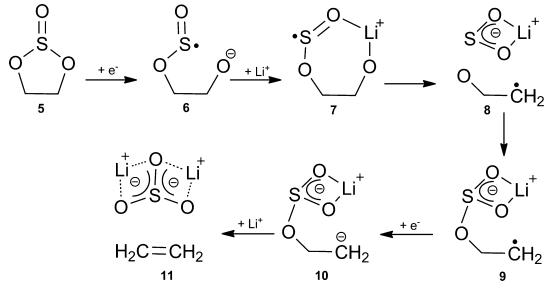

is also illustrated in Figure 3. In this mechanism, ES is directly reduced to give an open anion radical, which is then stabilized by Li^+ to form a relatively stable radical intermediate **7** that gives **9** through a transition state **8** with a barrier energy of 36.35 kcal/mol. A population density analysis on the spin density shows that the unpaired electron is totally shifted from the sulfur to carbon atom with a coefficient of 0.94.

Because the open-chain radical **9** is very reactive, it undergoes further reduction by the second electron transfer from the polarized electrode, causing the termination of the radical to give **10**. The stabilization of **10** by the addition of another Li^+ results in the formation of Li_2SO_3 and ethylene gas. However, in the one-electron reduction (similar to low current

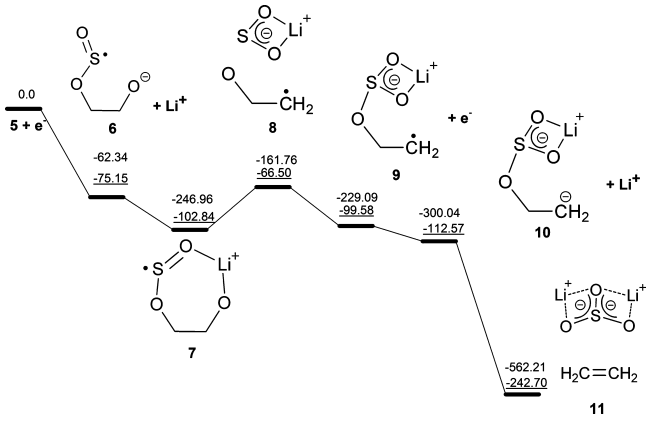

Figure 3. Potential energy (underlined data) and Gibbs Free energy profile for the two-electron reductive decomposition path of ES calculated with PCM-B3LYP/6-311++G(d,p).

density), the self-dissociation of **16** results in the formation of **18**, which is a weak complex of the unpaired nucleophilic sulphite anion ($LiSO_3^-$) and ethylene gas. $LiSO_3^-$, which can act as a good nucleophilic agent, would react with another solvated ES to give $(CH_2OSO_2Li)_2$ or with solvated PC to produce $CH_3CH(OSO_2Li)CH_2OCO_2Li$. It can also participate in an ion-paring reaction with Li^+ and precipitate as Li_2SO_3, as shown in Scheme 2. The relative energies for the one-electron

Scheme 2. One-Electron Reduction Mechanism of ES

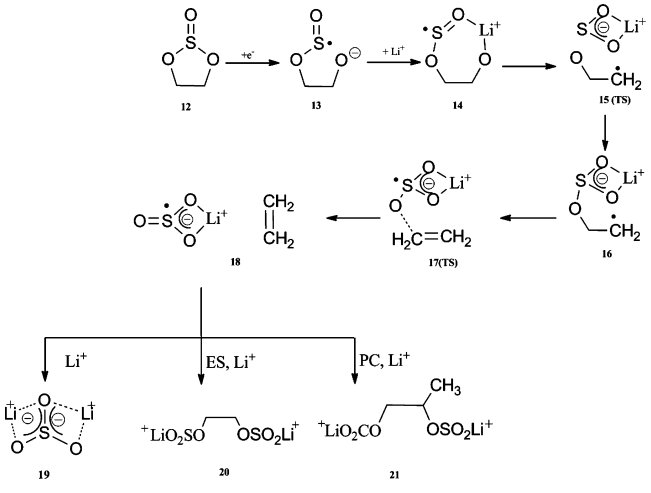

reduction of ES are shown in Table 6. As indicated in the energy surface profiles for one- and two-electron reduction mechanisms (Figures 4 and 3, respectively), the generation of the inorganic product is much more favorable in the two-electron reduction process than that in the one-electron process. From the thermodynamics point of view, Table 7 shows that the formation of $(CH_2OSO_2Li)_2$ and $CH_3CH(OSO_2Li)CH_2OCO_2Li$ is much favorable than the path leading to the formation of the inorganic product, Li_2SO_3. In addition to the ability of these species to improve the electrochemical performance when coated on the carbonaceous electrode, they were also identified as major components of the SEI, as reported elsewhere.[28,60]

We have also studied a similar mechanism in Scheme 3 to examine whether the reduction of Li^+(ES) is favored over the direct reduction of ES without first coordinating with Li^+. To

dx.doi.org/10.1021/jp3081996 | J. Phys. Chem. A 2012, 116, 11025−11033

Table 6. Relative Energies and Gibbs Free Energies (kcal/mol) for the One-Electron Reduction of ES

		ΔE	ΔG_{vac} [a]	ΔG_{sol} [b]
ES	12 + Li^+ + e^-	0.0	0.0	0.0
	13 + Li^+	−75.15	−23.39	−62.34 (−54.96)
	14	−102.84	−187.78	−246.96 (−239.58)
	15	−66.50	−138.79	−161.76 (−154.38)
	16	−99.60	−171.24	−229.09 (−221.71)
	17	−82.83	−161.89	−201.75 (−194.36)
	18	−100.30	−183.97	−243.43 (236.05)

[a] ΔG_{vac} stands for the relative Gibbs free energy in gas phase calculated with B3LYP/6-311++G(d,p). [b] $\Delta G_{sol} = \Delta G_{vac}$ + relative solvation free energies, including −37.59 kcal/mol for the free energy of solvation of electron in H_2O (ε=80.20) and values in parentheses are calculated using −44.97 kcal/mol for the free energy of solvation of electron in CH_3O (ε=33.0) from reference 59.

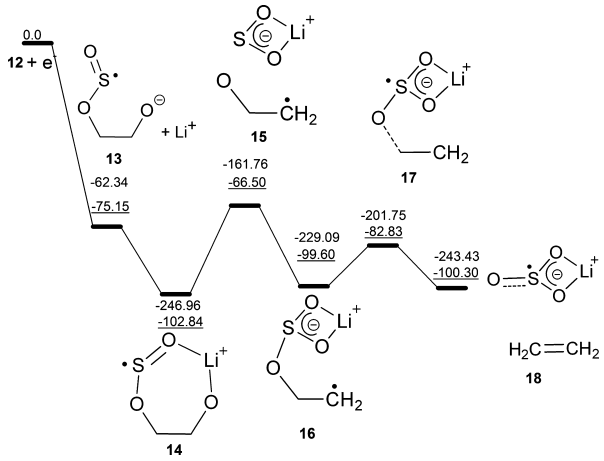

Figure 4. Potential energy (underlined data) and Gibbs Free energy profile for the one-electron reductive decomposition path of ES calculated with PCM-B3LYP/6-311++G(d,p).

Table 7. Gibbs Free Energies (ΔG, kcal/mol) for the Formation of Major Products from the Reaction of 24 with Solvent Molecules and with Li^+

reactants	products	ΔG
18 + Li^+	Li_2SO_3	−99.88
18 + ES + Li^+	$(CH_2OSO_2Li)_2$	−113.33
18 + PC + Li^+	$CH_3CH(OSO_2Li)CH_2OCO_2Li$	−103.05

Scheme 3. Two-Electron Reduction Mechanism of Li^+(ES)

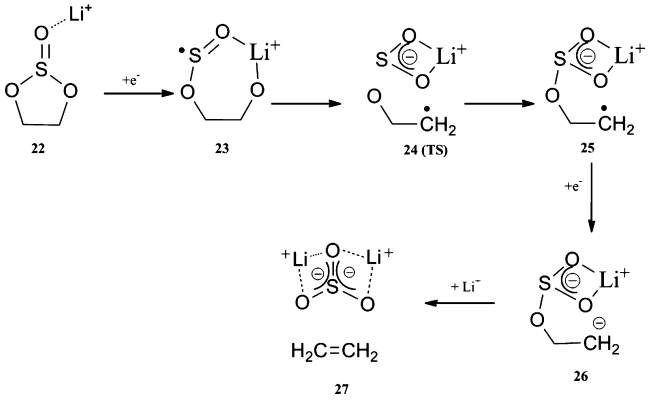

determine the electrochemical reduction potentials of different solvated species, a thermodynamic cycle[61] as shown in Figure 5

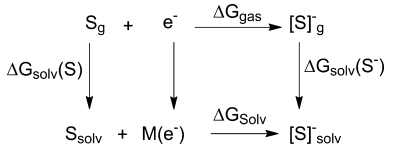

Figure 5. The thermodynamic cycle proposed for the calculation of the free energy of the reduction reaction ($S + e^- \rightarrow S^-$).

is employed to calculate the Gibbs free energy change for the reduction of solvated species (S). In this cycle, $\Delta G_{solv}(S)$ and $\Delta G_{solv}(S^-)$ are the solvation free energies of molecule S and its anion S^-, respectively, and ΔG_{gas} is the redox energy in the gas phase. These values are then used to calculate the overall reaction of the standard Gibbs free energy for the reduction reaction, as shown in eq 1.

$$\Delta G_{solv} = \Delta G_{solv}(S^-) + \Delta G_{gas} - \Delta G_{solv}(S) \quad (1)$$

The one-electron thermodynamic oxidation potential for the species versus Li/Li^+ can be then calculated using eq 2, which is derived from the Nernst equation, where 1.46 V is subtracted to account for the experimentally measured potential of the reference electrode.[62]

$$E^\circ_{red}[Li/Li^+] = \frac{-\Delta G_{solv}}{F} - 1.46\ V \quad (2)$$

The calculated reduction potentials for ES, Li^+(ES), PC, and Li^+(PC) are presented in Table 8 and compared with the

Table 8. Calculated and Experimental Reduction Potentials (V) for PC, ES, Li^+(ES), and Li^+(PC)

	E^0 (Reduction Potential in Solution)	
	calculated[a]	experimental
PC	1.57	1.0−1.6[b]
Li^+(PC)	1.81	1.0−1.6[b]
ES	1.90	1.8[c]
Li^+(ES)	2.05	1.8[c]

[a] The reduction potential of a molecule corresponds to the negative of the free energy for the formation (in eV) of M^- in solution divided by Faraday's constant (in eV) and subtracts 1.46 V to account for the Li/Li^+ reference electrode. [b] From ref 16. [c] From ref 30.

experimentally reported values. The reduction potential of ES is less than that of Li^+(ES) by 0.15 V and is in good agreement with the experimental value lying within 0.10 V of the reported result. The small variation from the experimentally reported results exists because the experimental reduction potentials are not the real thermodynamics potentials but are found by approximating the thermodynamic potentials based on kinetic measurements. This observation supports our claim that ES is directly reduced to an open anion structure without first coordinating with Li^+. Moreover, as shown in Table 5, the change in free energy of the final product **27** is less favorable by ~119 kcal/mol than that of **11** (−442.52 versus −562.21 kcal/mol).

Reduction Mechanism of (ES)Li^+(PC) and (ES)Li^+(PC)$_2$. The relative energies and other relevant data for the reductive decomposition of (PC)Li^+(ES) and (PC)$_2$$Li^+$(ES) are shown in Tables 9 and 10, respectively, and their profiles of the potential

dx.doi.org/10.1021/jp3081996 | J. Phys. Chem. A 2012, 116, 11025−11033

Table 9. Relative Energies,[a] Enthalpies, Free Energies (in kcal/mol), and SDs of the Stationary Points and Imaginary Frequencies (ω/cm^{-1}) of Transition States for the Reduction Process of (ES)Li$^+$(PC) Calculated with B3LYP/6-311++G(d,p)

structures	ΔE + ΔZPE	ΔH	ΔG	SD	ω
28	0	0	0	0	
29	−121.46 (−79.46)	−121.22	−121.63	S (0.59)	
30 (TS, 29 ↔ 31)	−80.01 (−42.88)	−79.86	−79.57		−854
31	−110.40 (−69.99)	−109.71	−110.73	C (0.97)	
32 (TS, 31 ↔ 33)	−100.26 (−60.18)	−99.72	−101.55		−519
33	−116.68 (−76.36)	−115.25	−119.05		

[a]The data in the parentheses are from PCM-B3LYP/6-311++G(d,p).

energy surface and Gibbs free energy surface are shown in Figures 6 and 7, respectively.

Table 10. Relative Energies, Enthalpies, Free Energies (in kcal/mol), and SDs of the Stationary Points and Imaginary Frequencies (ω/cm^{-1}) of Transition States for the (ES)Li$^+$(PC)$_2$ Reduction Process Calculated with B3LYP/6-311++G(d,p)

structures	ΔE + ΔZPE	ΔH	ΔG	SD	ω
34	0	0	0	0	
35	−108.86	−108.85	−106.25	S (0.59)	
36 (TS, 35 ↔ 37)	−76.41	−76.51	−71.85		−747.09
37	−98.46	−97.88	−95.49	C (0.98)	
38 (TS, 37 ↔ 39)	−88.62	−88.31	−85.34		−497.53
39	−107.92	−106.56	−107.23		

From the reaction mechanism points of view, both (PC)Li$^+$(ES) (**28**) and (PC)$_2$Li$^+$(ES) (**34**) undergo quite similar paths to give **33** and **39**, respectively, as the final products. On the basis of our calculations both in the gas phase and solution, **28** and **34** initially reduced to stable ion pair intermediates (**29** and **35**, respectively) by the reduction of ES. In both cluster models, the LUMO lies entirely on the ES particularly on the S−O bond. As a result of the filling up of the LUMO by the incoming electron, the S−O antibonding orbitals are occupied, and bond stretching is facilitated, leading to the opening of the ES ring. This finding is consistent with the NBO charge distribution, which shows that the additional electron is mainly located on the sulfur atom of the reduced species **29** and **35**, as shown in Table 9 and 10, respectively.

As a result of the explicit inclusion of solvent molecules, compared to the ES reduction intermediate **7**, the vertical electron affinities of **29** and **35** are significantly increased to 121.46 and 108.84 kcal/mol, respectively. Therefore, relative to the free ES, the cluster models have higher affinity to accept electrons. Moreover, the implicit solvent effect, as demonstrated by the PCM calculation, indicates a pronounced solvent effect in the reduction process, which is exhibited by further increase of the electron affinity. The seven-membered rings that are formed in one- and two-electron reduction of ES (**14** and **7**, respectively) are higher in energy when related to a similar ring formation in **29** and **35**. Hence, the extra stability of **29** and **35** can be attributed to the presence of one or more coordinated PC molecules. We can now conclude that ES can easily be reduced compared to the PC molecule in PC-based electrolyte systems of Li ion batteries.

As a result of the inner-sphere electron-transfer process, the stable radical intermediate **29** proceeds via a transition state **30** to give **31**. The located transition state has been confirmed by IRC calculations and the vibrational modes of its eigenvectors. From the NBO calculation, it can be seen that the unpaired electron is totally shifted from the sulfur atom of **29** to the carbon atom of the terminal −CH$_2$ in **31** with a coefficient of 0.97. This electron transfer is accompanied by the opening of the seven-membered ring to give a radical intermediate that is

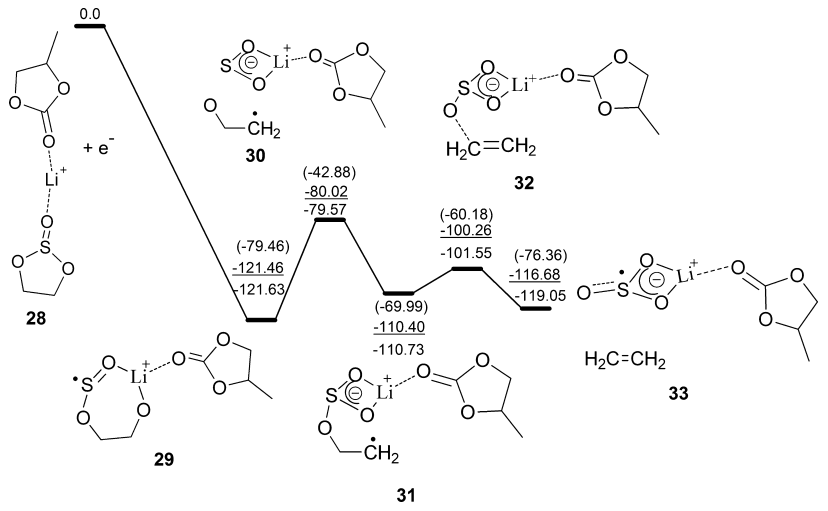

Figure 6. Potential energy (underlined data) and Gibbs Free energy profile for the one-electron reductive decomposition path of (ES)Li$^+$(PC) calculated with B3LYP/6-311++G(d,p). The data in parentheses refer to relative energies calculated with PCM-B3LYP/6-311++G(d,p).

dx.doi.org/10.1021/jp3081996 | J. Phys. Chem. A 2012, 116, 11025−11033

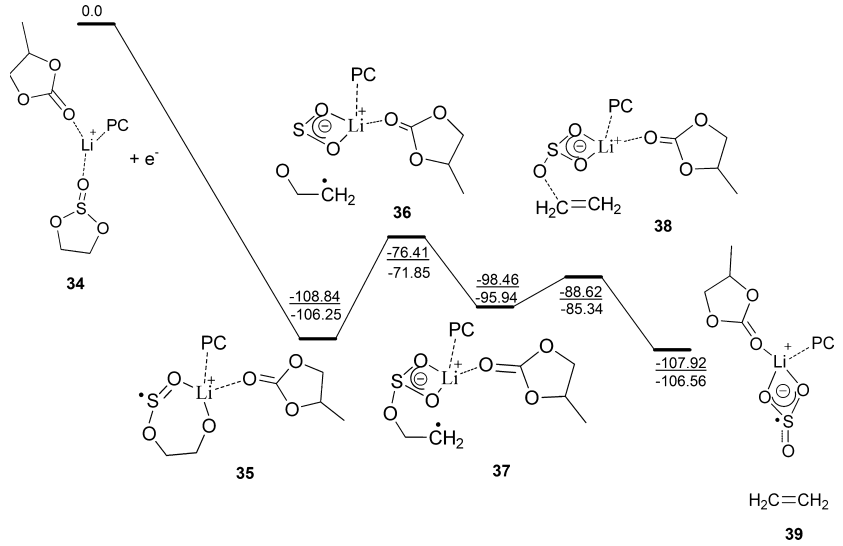

Figure 7. Potential energy (underlined data) and Gibbs Free energy profile for the one-electron reductive decomposition path of $(ES)Li^+(PC)_2$ calculated with B3LYP/6-311++G(d,p).

relatively higher in energy than the seven-membered ring. As a result of the stability induced by the extra PC molecule, the energy barrier for the formation of **37** is lower than that for the formation of **31** (32.45 versus 41.45 kcal/mol). The radical intermediates **31** and **37** undergo termination reactions to give **33** and **39**, respectively, which are weak complexes of ethylene gas and $ROSO_2Li$. It should be noted that $ROSO_2Li$ is experimentally reported as one of the components of the SEI film when ES is used as an electrolyte additive.[28,60]

On the basis of the above discussion, the protective-film-forming behavior of ES can be clarified by considering a relatively higher reduction potential of ES in PC-based electrolytes. The formation of the more stable seven-membered radical intermediates may help to overcome the higher barrier observed in the reactions **29** → **31** and **35** → **37**. Even though the interaction of the reduction products of ES with the surface of the electrode needs further work because of the lower lithium ion binding energy of **28** and **34** (Table 4) relative to PC (hence the reduction reactions mainly occur at the edge of the graphite), it is unlikely that ES co-intercalates in to the negative electrode. Moreover, as a result of the possible formation of a dense SEI film beforehand on the electrode surface by ES, the co-intercalation of PC into the crystal boundary that causes intergranular fracture can be avoided.

All of the above proposed good passivating species (Li_2SO_3, $ROSO_2Li$, $(CH_2OSO_2Li)_2$, and $CH_3CH(OSO_2Li)$-CH_2OCO_2Li) are compact and polar. Their passivating properties can be attributed to the possibility of good adhesion to the surface of the graphite electrode as a result of their inherent ionic structure and polarity. In addition to the conceivable presence of electrostatic interactions between the negatively charged electrode surface and lithium ions of this species, the presence of lithium-rich compact polycrystalline layer of inorganic species such as Li_2SO_3 could also facilitate Li ion diffusion though the protective film. It is believed that Li intercalation into a negative electrode (graphite) is composed of several successive processes, including the migration of the Li ion through the protective film followed by insertion into the carbon supported by charge transfer at the film−electrode interface and, finally, solid-state diffusion of lithium into the graphite.[51,63−65] We can speculate that as a result of the possible presence of interstitial sites in this lithium-rich solid ionic compounds, the diffusion of the lithium ion though the protective film will be facilitated.[66]

CONCLUSIONS

High-level density functional calculations have been carried out for ES and $(ES)Li^+(PC)_n$ (n = 0−2) to investigate the role of ES as a SEI-forming electrolyte additive of lithium ion batteries. It is found that ES in solvent is initially reduced prior to PC to give an open-chain radical, without first being coordinated with Li^+. This open-chain radical is then stabilized by dissolved lithium ion, resulting in a more stable intermediate releasing a large amount of energy. The subsequent electron-transfer reaction results in the generation of another intermediate that experiences further electron transfer or self-dissociation.

On the basis of the results presented here, it may be concluded that ES can undergo one- and two-electron reduction to give $(CH_2OSO_2Li)_2$, $CH_3CH(OSO_2Li)$-CH_2OCO_2Li, and Li_2SO_3 as the main products in which the generation of the inorganic product is much more favorable in the two-electron reduction process than that in the one-electron process. The significant improvement in the passivation of the graphite electrode in the presence of ES is attributed to the reductive decomposition of ES, $(ES)Li^+(PC)$, and $(ES)Li^+(PC)_2$. Therefore, the major products that are responsible for the generation of a protective SEI film are Li_2SO_3, $(CH_2OSO_2Li)_2$, $CH_3CH(OSO_2Li)CH_2OCO_2Li$, and $ROSO_2Li$.

ASSOCIATED CONTENT

Supporting Information

The optimized geometries of the possible species formed during the reductive decomposition of PC-based electrolyte containing ES as an electrolyte additive. This material is available free of charge via the Internet at http://pubs.acs.org.

AUTHOR INFORMATION

Corresponding Author

*Tel.: +886 2 2737 6653. Fax: +886 2 2737 6644. E-mail: jcjiang@mail.ntust.edu.tw.

Notes

The authors declare no competing financial interest.

■ ACKNOWLEDGMENTS

This work was supported by the National Science Council of Taiwan (NSC-100-3113-E-011-002) and the Ministry of Economic Affairs of Taiwan (101-EC-17-A-08-S1-183). We are also grateful to the National Center of High-Performance Computing for computer time and facilities.

■ REFERENCES

(1) Jansen, A. N.; Kahaian, A. J.; Kepler, K. D.; Nelson, P. A.; Amine, K.; Dees, D. W.; Vissers, D. R.; Thackeray, M. M. *J. Power Sources* **1999**, *81*, 902−905.
(2) Scrosati, B. *Electrochim. Acta* **2000**, *45*, 2461−2466.
(3) Scrosati, B. *J. Solid State Electrochem.* **2011**, *15*, 1623−1630.
(4) Megahed, S.; Ebner, W. *J. Power Sources* **1995**, *54*, 155−162.
(5) Tarascon, J. M.; Armand, M. *Nature* **2001**, *414*, 359−367.
(6) Schalkwijk, W.; Scrosati, B. In *Advances in Lithium-Ion Batteries*; Schalkwijk, W., Scrosati, B., Eds.; Springer: New York, 2002; pp 1−5.
(7) Peled, E. *J. Electrochem. Soc.* **1979**, *126*, 2047−2051.
(8) Xu, K. *Chem. Rev.* **2004**, *104*, 4303−4418.
(9) Arakawa, M.; Yamaki, J.-i. *J. Power Sources* **1995**, *54*, 250−254.
(10) Chung, G.-C.; Kim, H.-J.; Yu, S.-I.; Jun, S.-H.; Choi, J.-w.; Kim, M.-H. *J. Electrochem. Soc.* **2000**, *147*, 4391−4398.
(11) Inaba, M.; Siroma, Z.; Kawatate, Y.; Funabiki, A.; Ogumi, Z. *J. Power Sources* **1997**, *68*, 221−226.
(12) Billaud, D.; Naji, A.; Willmann, P. *J. Chem. Soc., Chem. Commun.* **1995**, 1867−1868.
(13) Spahr, M. E.; Palladino, T.; Wilhelm, H.; Wursig, A.; Goers, D.; Buqa, H.; Holzapfel, M.; Novak, P. *J. Electrochem. Soc.* **2004**, *151*, A1383−A1395.
(14) Dey, A. N.; Sullivan, B. P. *J. Electrochem. Soc.* **1970**, *117*, 222−224.
(15) Xu, K. *J. Electrochem. Soc.* **2009**, *156*, A751−A755.
(16) Zhang, X.; Kostecki, R.; Richardson, T. J.; Pugh, J. K.; Ross, J. P. N. *J. Electrochem. Soc.* **2001**, *148*, A1341−A1345.
(17) Ohtani, H.; Hirao, Y.; Ito, A.; Tanaka, K.; Hatozaki, O. *J. Therm. Anal. Calorim.* **2009**, *99*, 139−144.
(18) Wang, Y.; Balbuena, P. B. *J. Phys. Chem. B* **2002**, *106*, 4486−4495.
(19) Endo, E.; Tanaka, K.; Sekai, K. *J. Electrochem. Soc.* **2000**, *147*, 4029−4033.
(20) Zhang, S. S. *J. Power Sources* **2006**, *162*, 1379−1394.
(21) Yao, W.; Zhang, Z.; Gao, J.; Li, J.; Xu, J.; Wang, Z.; Yang, Y. *Energy Environ. Sci.* **2009**, *2*, 1102−1108.
(22) Xing, L.; Li, W.; Xu, M.; Li, T.; Zhou, L. *J. Power Sources* **2011**, *196*, 7044−7047.
(23) Ein-Eli, Y.; Thomas, S. R.; Koch, V. R. *J. Electrochem. Soc.* **1996**, *143*, L195−L197.
(24) Chen, R.; Wu, F.; Li, L.; Guan, Y.; Qiu, X.; Chen, S.; Li, Y.; Wu, S. *J. Power Sources* **2007**, *172*, 395−403.
(25) Xu, M. Q.; Li, W. S.; Zuo, X. X.; Liu, J. S.; Xu, X. *J. Power Sources* **2007**, *174*, 705−710.
(26) Ein-Eli, Y.; Thomas, S. R.; Koch, V. R. *J. Electrochem. Soc.* **1997**, *144*, 1159−1165.
(27) Yu, B. T.; Qiu, W. H.; Li, F. S.; Cheng, L. *J. Power Sources* **2006**, *158*, 1373−1378.
(28) Ota, H.; Sato, T.; Suzuki, H.; Usami, T. *J. Power Sources* **2001**, *97*−*98*, 107−113.
(29) Jeong, S.-K.; Inaba, M.; Mogi, R.; Iriyama, Y.; Abe, T.; Ogumi, Z. *Langmuir* **2001**, *17*, 8281−8286.
(30) Wrodnigg, G. H.; Besenhard, J. O.; Winter, M. *J. Electrochem. Soc.* **1999**, *146*, 470−472.
(31) Han, Y.-K.; Lee, S. U.; Ok, J.-H.; Cho, J.-J.; Kim, H.-J. *Chem. Phys. Lett.* **2002**, *360*, 359−366.
(32) Frisch, M. J.; Trucks, G. W.; Schlegel, H. B.; Scuseria, G. E.; Robb, M. A.; Cheeseman, J. R.; Montgomery, J., J. A.; Vreven, T.; Kudin, K. N.; Burant, J. C.et al. *Gaussian 03*, revision D.02; Gaussian Inc.: Wallingford, CT, 2004.
(33) Lee, C.; Yang, W.; Parr, R. G. *Phys. Rev. B* **1988**, *37*, 785−789.
(34) Becke, A. D. *J. Chem. Phys.* **1993**, *98*, 5648.
(35) Stephens, P. J.; Devlin, F. J.; Chabalowski, C. F.; Frisch, M. J. *J. Phys. Chem.* **1994**, *98*, 11623−11627.
(36) Vosko, S. H.; W., L.; Nusair, M. *Can. J. Phys.* **1980**, *58*, 1200−1211.
(37) Frisch, M. J.; Pople, J. A.; Binkley, J. S. *J. Chem. Phys.* **1984**, *80*, 3265−3269.
(38) Xu, M.; Liu, Y.; Li, B.; Li, W.; Li, X.; Hu, S. *Electrochem. Commun.* **2012**, *18*, 123−126.
(39) Li, B.; Xu, M.; Li, T.; Li, W.; Hu, S. *Electrochem. Commun.* **2012**, *17*, 92−95.
(40) Xu, M.; Zhou, L.; Hao, L.; Xing, L.; Li, W.; Lucht, B. L. *J. Power Sources* **2011**, *196*, 6794−6801.
(41) Xu, M.; Hao, L.; Liu, Y.; Li, W.; Xing, L.; Li, B. *J. Phys. Chem. C* **2011**, *115*, 6085−6094.
(42) Li, T.; Xing, L.; Li, W.; Peng, B.; Xu, M.; Gu, F.; Hu, S. *J. Phys. Chem. A* **2011**, *115*, 4988−4994.
(43) Leggesse, E. G.; Jiang, J. C. *RSC Adv.* **2012**, *2*, 5439−5446.
(44) Reed, A. E.; Weinstock, R. B.; Weinhold, F. *J. Chem. Phys.* **1985**, *83*, 735−746.
(45) Barone, V.; Cossi, M. *J. Phys. Chem. A* **1998**, *102*, 1995.
(46) Bader, R. F. W. *Atoms in Molecules — A Quantum Theory*; Oxford University Press: Oxford, U.K., 1990.
(47) Bu, Y.; Liu, Y.; Deng, C. *J. Mol. Struct.: THEOCHEM* **1998**, *422*, 219−228.
(48) Robertson, W. D.; Hammer, N. I.; Bartmess, J. E.; Compton, R. N.; Diri, K.; Jordan, K. D. *J. Chem. Phys.* **2005**, *122*, 204319.
(49) Kobayashi, S.; Uchimoto, Y. *J. Phys. Chem. B* **2005**, *109*, 13322−13326.
(50) Sagane, F.; Abe, T.; Ogumi, Z. *J. Phys. Chem. C* **2009**, *113*, 20135−20138.
(51) Xu, K.; von Cresce, A.; Lee, U. *Langmuir* **2010**, *26*, 11538−11543.
(52) Bhatt, M. D.; Cho, M.; Cho, K. *Appl. Surf. Sci.* **2010**, *257*, 1463−1468.
(53) Park, M. H.; Lee, Y. S.; Lee, H.; Han, Y.-K. *J. Power Sources* **2011**, *196*, 5109−5114.
(54) Matsuda, Y.; Fukushima, T.; Hashimoto, H.; Arakawa, R. *J. Electrochem. Soc.* **2002**, *149*, A1045−A1048.
(55) Fukushima, T.; Matsuda, Y.; Hashimoto, H.; Arakawa, R. *Electrochem. Solid-State Lett.* **2001**, *4*, A127−A128.
(56) Fukushima, T.; Matsuda, Y.; Hashimoto, H.; Arakawa, R. *J. Power Sources* **2002**, *110*, 34−37.
(57) Jarek, R. L.; Miles, T. D.; Trester, M. L.; Denson, S. C.; Shin, S. K. *J. Phys. Chem. A* **2000**, *104*, 2230−2237.
(58) Spångberg, D.; Hermansson, K. *Chem. Phys.* **2004**, *300*, 165−176.
(59) Vollmer, J. M.; Curtiss, L. A.; Vissers, D. R.; Amine, K. *J. Electrochem. Soc.* **2004**, *151*, A178−A183.
(60) Ota, H.; Akai, T.; Namita, H.; Yamaguchi, S.; Nomura, M. *J. Power Sources* **2003**, *119*−*121*, 567−571.
(61) Roy, L. E.; Jakubikova, E.; Guthrie, M. G.; Batista, E. R. *J. Phys. Chem. A* **2009**, *113*, 6745−6750.
(62) Trasatti, S. *Pure Appl. Chem.* **1986**, *58*, 955−966.
(63) Wang, F.; Graetz, J.; Moreno, M. S.; Ma, C.; Wu, L.; Volkov, V.; Zhu, Y. *ACS Nano* **2011**, *5*, 1190−1197.
(64) Christensen, J.; Newman, J. *J. Electrochem. Soc.* **2004**, *151*, A1977−A1988.
(65) Persson, K.; Sethuraman, V. A.; Hardwick, L. J.; Hinuma, Y.; Meng, Y. S.; van der Ven, A.; Srinivasan, V.; Kostecki, R.; Ceder, G. *J. Phys. Chem. Lett.* **2010**, *1*, 1176−1180.
(66) Xu, K.; von Cresce, A. *J. Mater. Chem.* **2011**, *21*, 9849−9864.